

Spin-Orbit Coupling-Driven Chirality Switching of Spin Waves in Altermagnets

Wen-Tong Li^{1,2}, Yu-Biao Wu¹, Lin Zhuang^{3*}, Jian-Tao Wang^{1,2,4},
Wu-Ming Liu^{1,2*}

¹Beijing National Laboratory for Condensed Matter Physics and
Institute of Physics, Chinese Academy of Sciences, Beijing, 100190,
China.

²School of Physical Sciences, University of Chinese Academy of
Sciences, Beijing, 100049, China.

³School of Physics, Sun Yat-Sen University, Guangzhou, 510275, China.

⁴Songshan Lake Materials Laboratory, Dongguan, Guangdong, 523808,
China.

*Corresponding author(s). E-mail(s): stszhl@mail.sysu.edu.cn;
wmliu@iphy.ac.cn;

Abstract

Chirality of spin waves offers an advantageous binary carrier for data transmission and processing with ultrafast dynamics and low power consumption. Altermagnets possess intrinsic chirality-splitting spin waves and vanishing net magnetization, thus emerging as ideal platforms to host chirality bits. However, active control of the chiral states remains a key challenge for realizing logic operations in chirality-based circuits. Here, we propose a novel scheme for reversibly switching spin-wave chirality in altermagnets between right- and left-handedness by tuning spin-orbit coupling (SOC) strength. Specifically, for in-plane spin polarization, SOC hybridizes with the altermagnetism, which induces a momentum-dependent competition. The chirality-splitting structure of spin waves is dominated by either SOC or altermagnetism in different Brillouin zone regions, allowing chirality switching by altering their relative strength. An experimental design utilizing an antiferromagnetic substrate to induce SOC and a heavy-metal stripe for chirality detection is proposed. Our work establishes a novel pathway for controlling spin-wave chirality in altermagnets via SOC, laying the groundwork for developing spintronic devices utilizing switchable chiral spin waves as dynamic information carriers.

Within the classification of non-relativistic spin groups [1, 2], altermagnets represent a third fundamental class of collinear magnets, alongside ferro- and antiferromagnets. They are characterized by sublattices connected via time reversal combined with mirror or rotation symmetries, which leads to spin-resolved structures [1–11] in both real and momentum spaces. A growing number of materials, including MnTe [3, 5], CrSb [6, 7], and KV₂Se₂O [8] have been experimentally identified as altermagnets, motivating explorations of emergent phenomena [12] such as charge-spin conversion [13–15], magneto-optical effects [16, 17], tunneling magnetoresistance [18, 19] and anomalous thermal transport [20]. Particularly promising for spintronics are their spin transport properties [21–25]. Notably, spin-wave excitations in altermagnets exhibit anisotropic transport [21, 23] and intrinsic chirality splitting [22, 25] absent in conventional antiferromagnets. Chirality emerges as a novel information carrier, independent of charge and spin, where left-handed (LH) and right-handed (RH) states naturally encode binary digits, enabling information processing via chirality bits. While the inherent chirality splitting positions altermagnets as ideal platforms for chirality-bit operations, achieving controllable switching of spin-wave chirality remains a fundamental challenge.

Existing methods, reliant on varying excitation frequency or external magnetic fields [26, 27], may excite unintended modes, limit switching speed, and hinder nanoscale integration. Consequently, new mechanisms enabling precise, high-speed chirality switching are essential. Spin-orbit coupling (SOC), the relativistic interaction between an electron’s spin and orbital motion, provides a powerful pathway for magnetic control [28–30]. It profoundly influences magnetic anisotropy [31, 32] and governs spin relaxation and transport dynamics [28, 33, 34] in conventional magnets. The interplay between relativistic SOC and non-relativistic altermagnetism yields novel phenomena, such as polarization-dependent anomalous Hall effects [35–40] arising from SOC-induced symmetry reduction [41, 42]. Nevertheless, the potential of SOC for dynamically manipulating spin-wave chirality in altermagnets, specifically achieving active chirality switching, remains unexplored.

In this article, we propose a mechanism for reversible switching of spin-wave chirality at specific frequency and momentum in altermagnets, achieved by tuning SOC strength. Employing non-equilibrium quantum field theory, we derive the effective action for a d-wave altermagnet with Rashba SOC, enabling systematic analysis of its magnetism and spin-wave excitations. For in-plane spin polarization, electronic band structure reveals hybridization between SOC and altermagnetism, underlying the asymmetric chirality-splitting structure of spin waves. Crucially, differing symmetries cause SOC and altermagnetic effects to cooperate or compete in distinct momentum directions, where the latter leads to chirality inversion. Leveraging this inversion, continuous SOC tuning enables reversible switching between LH and RH spin-wave modes. We also design an experimental protocol, using an antiferromagnetic substrate to generate tunable SOC and a heavy-metal stripe for chirality detection, to realize SOC-driven chirality switching. These results establish SOC as a powerful tool for manipulating chiral excitations in altermagnets and, more significantly, provide controlled switching of chirality bits on specific modes, laying the groundwork for chirality-based spintronic devices.

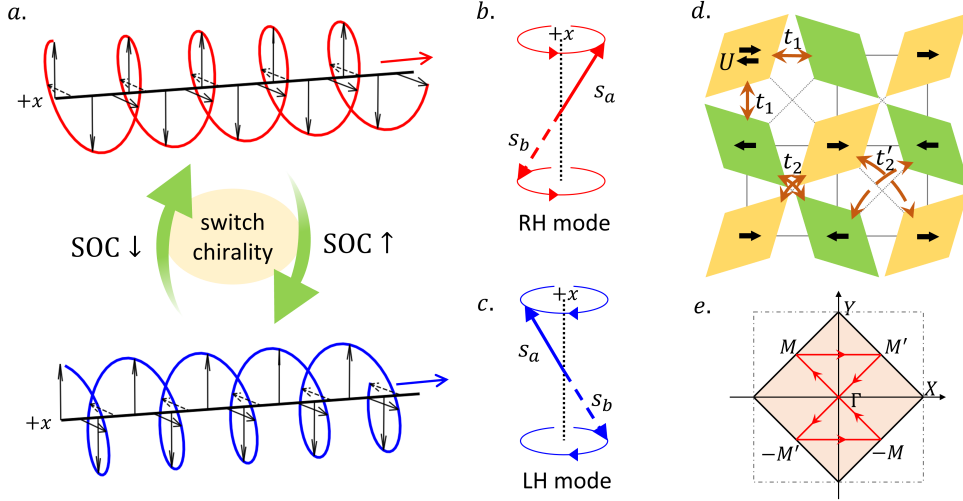


Fig. 1 Schematics of SOC-driven chirality switching. **a** The stable chirality of the spin-wave mode is switched by tuning SOC strength. The right-handed (RH) spin wave propagating towards $-x$ direction is switched to a left-handed (LH) one upon increasing SOC strength and such a process is reversible. Black arrows illustrate projected spin precession at specific moment on each site. The chirality is defined by the precessing direction of spins. From $+x$ perspective, the RH mode **(b)** exhibits a counter-clockwise precession while the LH mode **(c)** exhibits a clockwise one. s_a, s_b represent opposite spins on different sublattices A and B. **d** Real-space lattice configuration. The nearest-neighbor hopping t_1 , next-nearest-neighbor hopping t_2/t_2' and on-site repulsive interaction U are included. **e** Reduced Brillouin zone and high-symmetry path.

Effective action of the altermagnet with SOC

We consider a thin altermagnetic film coupled to an antiferromagnetic substrate, where broken structural inversion symmetry in the latter induces a Rashba SOC [28, 43] within the altermagnet. The system is described by the Hamiltonian

$$\begin{aligned}
 H = & -t_1 \sum_{\langle ij \rangle} (a_i^\dagger b_j + \text{h.c.}) - \sum_{\langle\langle ij \rangle\rangle \in d_1} (t_2 a_i^\dagger a_j + t_2' b_i^\dagger b_j) - \sum_{\langle\langle ij \rangle\rangle \in d_2} (t_2' a_i^\dagger a_j + t_2 b_i^\dagger b_j) \\
 & + U \sum_i (n_{i\uparrow}^a n_{i\downarrow}^a + n_{i\uparrow}^b n_{i\downarrow}^b) + i\lambda_R \sum_{\langle ij \rangle} (a_i^\dagger [\hat{e}_z \cdot (\vec{\sigma} \times \vec{d}_{ij})] b_j + \text{h.c.}), \quad (1)
 \end{aligned}$$

where $a^\dagger(a)$ and $b^\dagger(b)$ are creation (annihilation) operators of electrons on sublattices A and B, respectively. The first line contains an isotropic nearest-neighbor hopping of strength t_1 , and two anisotropic next-nearest-neighbor hopping, whose amplitude is $t_2(t_2')$ for A (B) sublattice along $d_1 = \pm(1, 1)$ and interchanged along $d_2 = \pm(1, -1)$. The anisotropic configuration makes different sublattices connected by rotation symmetry, which is the characteristic of altermagnets. We set $t_1 = 1$ as the energy unit in calculation. U is the repulsive Hubbard interaction, and λ_R describes the strength

of Rashba SOC. \hat{e}_z is the unit vector in z direction. $\vec{\sigma} = (\sigma^1, \sigma^2, \sigma^3)$ are Pauli matrices acting on spin space. \vec{d}_{ij} represents the connecting vector from lattice j to i . We also define a quantity $\delta = (t_2 - t'_2)/(t_2 + t'_2)$ to measure the magnitude of anisotropy. When $\delta = 0$, the altermagnet is reduced to a conventional antiferromagnet.

By Fourier transforming, the non-interacting Hamiltonian acquires the form $H_0 = \sum_k \Psi_k^\dagger h_0(k) \Psi_k$ in the basis $\Psi_k = (a_{k\uparrow}, b_{k\uparrow}, a_{k\downarrow}, b_{k\downarrow})^T$, where $h_0(k) = \varepsilon_0(k)\Gamma_{00} + \varepsilon_1(k)\Gamma_{01} + \varepsilon_2(k)\Gamma_{03} + \varepsilon_3(k)\Gamma_{11} + \varepsilon_4(k)\Gamma_{21}$, and $\Gamma_{\mu\nu} = \sigma^\mu \otimes \tau^\nu$ is the direct product of Pauli matrices in spin space and sublattice space. The band parameters are $\varepsilon_0(k) = -2(t_2 + t'_2) \cos k_x \cos k_y$, $\varepsilon_1(k) = -2t_1(\cos k_x + \cos k_y)$, $\varepsilon_2(k) = 2(t_2 - t'_2) \sin k_x \sin k_y$, $\varepsilon_3(k) = 2\lambda_R \sin k_y$, $\varepsilon_4(k) = -2\lambda_R \sin k_x$. Among these terms, ε_0 and ε_1 respect the highest symmetries in momentum space, including C_{4z} , C_{2x} and C_{2y} . The effect of anisotropy manifests itself in ε_2 , which preserves only $C_{4z}\mathcal{T}$. SOC terms ε_3 and ε_4 break the rotation symmetry down to C_{2y} and C_{2x} , respectively. Diagonalizing $h_0(k)$ yields the non-interacting bands

$$E_0 = \varepsilon_0 \pm \sqrt{|\varepsilon|^2 \pm 2\sqrt{\varepsilon_1^2(\varepsilon_3^2 + \varepsilon_4^2)}}, \quad (2)$$

where $|\varepsilon|^2 = \varepsilon_1^2 + \varepsilon_2^2 + \varepsilon_3^2 + \varepsilon_4^2$. The quadratic form under the nested square root reflects the restoration of the highest symmetry even in the presence of SOC, and highlights how Rashba SOC lifts the residual spin degeneracy whenever $\varepsilon_1 \neq 0$.

We then construct an effective action from the Hamiltonian. Through Hubbard-Stratonovich transformation, the interaction is decoupled by introducing two bosonic vector fields \vec{m}_A/\vec{m}_B on each sublattice. Due to the constraint of vanishing net magnetization, one of them can be eliminated by defining $\vec{m} = \vec{m}_A = -\vec{m}_B$ [44]. After integrating out the fermions, the effective action reads (see Supplementary Note 1)

$$S_{\text{eff}} = -i \text{Tr} \ln \left[\begin{pmatrix} G^R & G^K \\ 0 & G^A \end{pmatrix}^{-1} + \begin{pmatrix} m_c^i \Gamma_{i3} & m_q^j \Gamma_{j3} \\ m_q^j \Gamma_{j3} & m_c^i \Gamma_{i3} \end{pmatrix} \right] - \frac{12}{U} \int dx [\vec{m}_0(x) + \vec{m}_c(x)] \cdot \vec{m}_q(x), \quad (3)$$

where $x = (\vec{r}, t)$ is combined spacetime coordinates and $i, j \in \{1, 2, 3\}$ are spatial indices. G represents the dressed Green's function of electrons, which has a simple form in momentum-frequency space. The retarded (advanced) component is $G^{R/A}(k, \omega) = [\omega \pm i0 - h_0(k) + m_0^i \Gamma_{i3}]^{-1}$ and the Keldysh component is $G^K(k, \omega) = F(\omega)[G^R(k, \omega) - G^A(k, \omega)]$, with $F(\omega)$ the equilibrium fermionic distribution. $\vec{m}_c(\vec{m}_q)$ denotes the classical (quantum) Keldysh component and \vec{m}_0 is the finite part separated from \vec{m}_c . The static field \vec{m}_0 sets the altermagnetic order, while the infinitesimal fluctuations \vec{m}_c and \vec{m}_q govern the collective spin wave excitations. Eq. (3) provides the starting point for our analysis of altermagnetism and spin dynamics.

Electronic Band Structure

The equilibrium state is supposed to satisfy the stationary condition $\left. \frac{\delta S_{\text{eff}}}{\delta m_q} \right|_{m_q=0} = 0$. Taking the functional derivative of Eq. (3), we obtain the expectation value of the

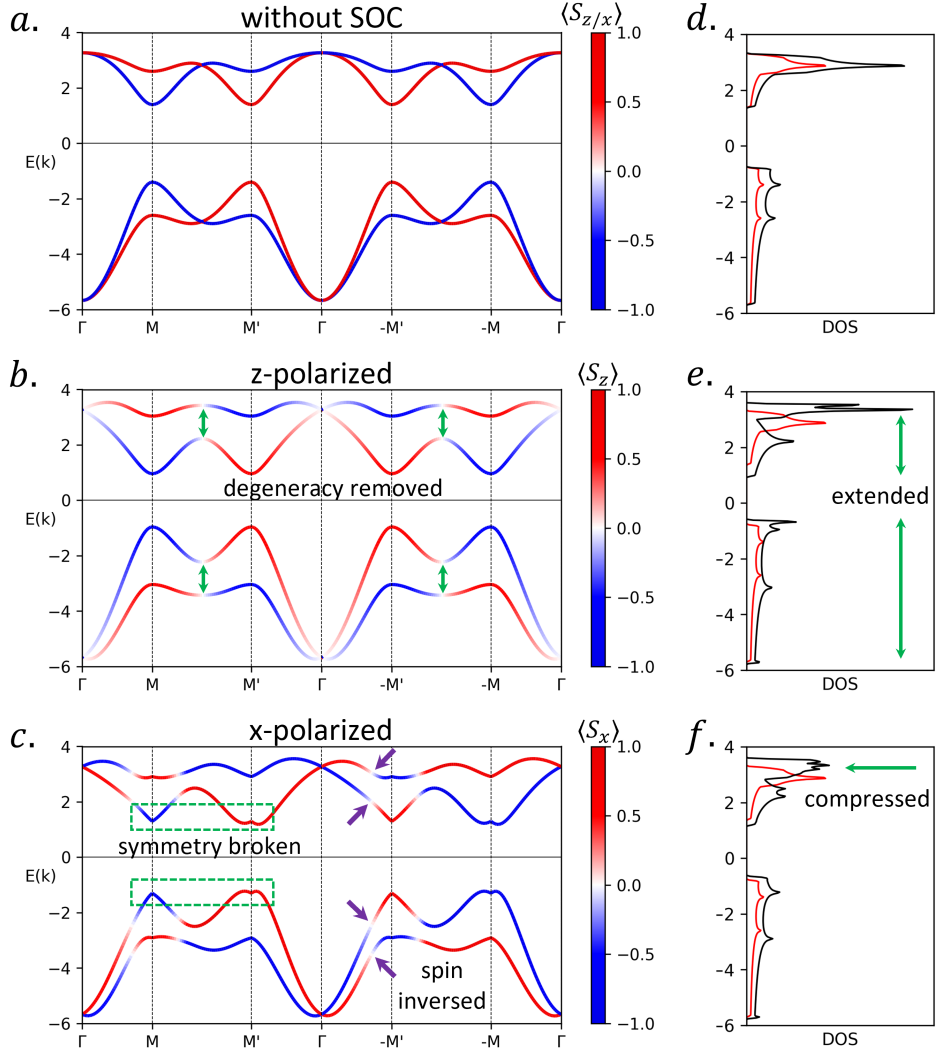


Fig. 2 Spin-projected electronic bands and density of states. **a** Altermagnetic bands without SOC. Spin-up and spin-down bands are well separated except high-symmetry paths $X - \Gamma - (-X)$ and $Y - \Gamma - (-Y)$. The polarization orientation respects $O(3)$ rotation symmetry and thus the same for S_z and S_x projection. **b** Bands with SOC $\lambda_R = 0.3$ and z polarization. The degeneracy along high-symmetry paths is removed, and the two spins are mixed in bands. **c** Bands with SOC $\lambda_R = 0.3$ and x polarization. The $C_{4z}\mathcal{T}$ symmetry in momentum space is broken while C_{2x} maintains. In $\Gamma - M$ and $\Gamma - (-M')$ ranges, a spin inversion appears, indicating competition between SOC and altermagnetism. **d-f** Density of states (DOS) corresponding to **(a-c)**. The red lines show spin-up contribution without SOC for comparison. **d** The contribution from spin-up and spin-down electrons are the same and the total DOS is simply twice the value of either. **e** The range of DOS extends to both sides. **f** The peak of DOS is compressed due to the misplacement of the two spin components.

order parameter

$$\langle m_0^i \rangle = -i \frac{U}{12} \text{Tr}[G^K \Gamma_{i3}], \quad (4)$$

which needs to be solved self-consistently (see Supplementary Note 2). For simplicity, we assume \vec{m}_0 is a constant and takes the form $\vec{m}_0 = m_0(\sin \theta \cos \phi, \sin \theta \sin \phi, \cos \theta)$ in spherical coordinates. $\theta = 0$ represents spins polarized perpendicular to the plane while $\theta = \frac{\pi}{2}$ in the plane. We restrict ourselves to the half-filling case and perform a numerical calculation. The result in the absence of SOC agrees with the mean-field study of Ref. [9] upon rescaling $\tilde{U} = \frac{2}{3}U$, which is caused by extending the spin degree of freedom into 3-dimension to generate in-plane polarization. Once \vec{m}_0 is determined, the interacting Hamiltonian becomes $h(k) = h_0(k) - m_0^i \Gamma_{i3}$.

For perpendicular polarization, $\vec{m}_0 = m_0 \hat{e}_z$, the band energies are

$$E_z = \varepsilon_0 \pm \sqrt{|\varepsilon|^2 + m_0^2 \pm 2\sqrt{\varepsilon_1^2(\varepsilon_3^2 + \varepsilon_4^2) + m_0^2(\varepsilon_2^2 + \varepsilon_3^2 + \varepsilon_4^2)}}. \quad (5)$$

The m_0 term under the outer root sign opens a gap between valence bands and conduction bands, and the one under the inner root sign lifts the degeneracy of spins. Due to the quadratic form, the splitting from SOC and altermagnetic order is always enhanced while preserving the highest momentum symmetry. As Fig. 2a shows, the bands without SOC exhibits spin splitting except at high-symmetry paths $X - \Gamma - (-X)$ and $Y - \Gamma - (-Y)$, where $\varepsilon_2 = 0$. There is a $C_{4z}\mathcal{T}$ symmetry between the two spins, which causes the total density of states (DOS) simply twice the value of spin-up (spin-down) component. With SOC on (Fig. 2b), the degeneracy along high-symmetry paths is removed, and the two spins are mixed up in every band, while the $C_{4z}\mathcal{T}$ symmetry still holds. The enhanced band splitting results in the extension of DOS.

However, when we polarize spins along x-axis, the energies become

$$E_x = \varepsilon_0 \pm \sqrt{|\varepsilon|^2 + m_0^2 \pm 2\sqrt{\varepsilon_1^2(\varepsilon_3^2 + \varepsilon_4^2) + m_0^2(\varepsilon_2^2 + \varepsilon_4^2) - 2m_0\varepsilon_1\varepsilon_2\varepsilon_3}}. \quad (6)$$

Apart from the quadratic terms, a hybridization term $-m_0\varepsilon_1\varepsilon_2\varepsilon_3$ arises under the inner root sign. It contains the linear factor $-\sin k_x$ and is not necessarily positive. The original spin splitting can be enhanced or suppressed depending on the sign of k_x . This term highlights the interplay of interaction, anisotropy and SOC, which vanishes if any ingredient is set to zero. Fig. 2c illustrates that the $C_{4z}\mathcal{T}$ symmetry is broken to C_{2x} by x polarization, reshaping the band structures. Notably, a spin inversion emerges in $\Gamma - M$ and $\Gamma - (-M')$ ranges, which indicates the competition between SOC and altermagnetism. The SOC-dominated spin structure around Γ is opposite to altermagnetism-dominated one around $M(-M')$. As a result of the symmetry breaking, the peaks of DOS for the two spins acquire a misplacement and the total maximum value is compressed to a half.

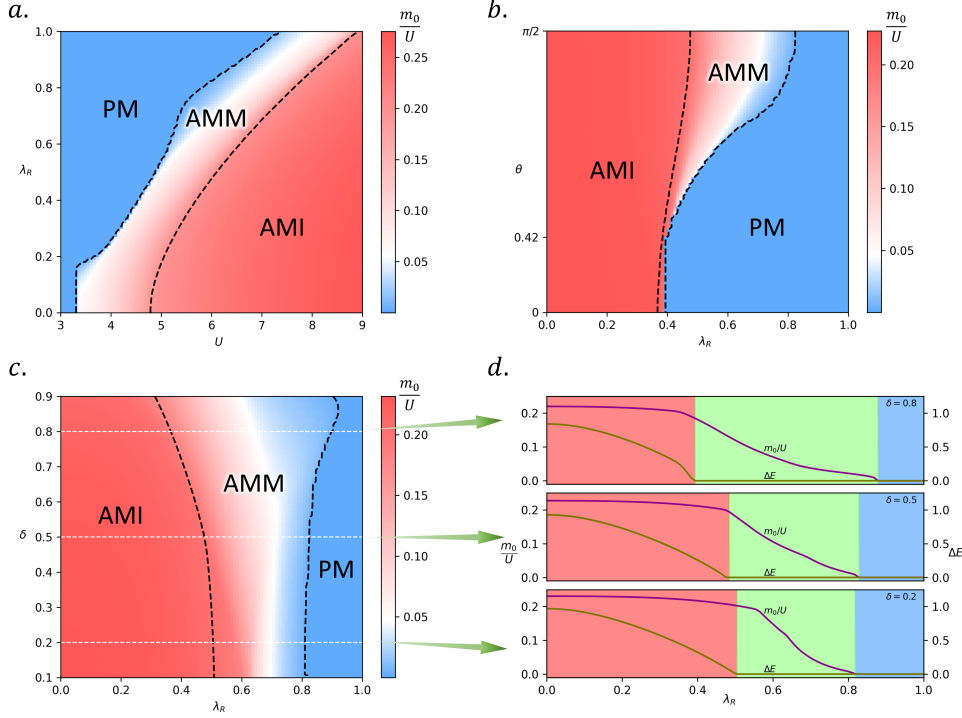


Fig. 3 Phase diagrams. According to the existence of altermagnetic order and energy gap, the areas are divided into altermagnetic insulator (AMI), altermagnetic metal (AMM) and paramagnetic metal (PM). **a** With SOC increasing, the altermagnetic region shrinks rapidly. **b** At small angle $\theta \lesssim 0.42$, the magnetic phase border is robust to the deviation from z-axis. As θ approaches $\frac{\pi}{2}$, the deflecting effect from SOC is weakened, and the intermediate AMM phase expands. **c** The rise of anisotropy δ promotes altermagnetic order but reduces the insulator region slightly. Three line cuts at $\delta = 0.2, 0.5, 0.8$ are correspondingly plotted in **(d)**. **d** Green lines show energy gap ΔE and purple lines are order parameters. The left borders are identified by $\Delta E = 0$ while the right ones by vanishing order parameters. As δ increases, the slope of the $\frac{m_0}{U}$ curve becomes gentle, corresponding to the expansion of AMM region. **(b-d)** are calculated at $U = 6$.

Stability of Altermagnetism

Since SOC plays the role of an effective magnetic field, it has influence on the orientation of spins, so that modifies the altermagnetic order. To make it explicit, we map out the magnetic phase diagrams by solving the self-consistent condition Eq. (4) across the parameter space of interaction U , SOC strength λ_R , polarization angle θ and anisotropy δ . The dependence on hopping strength $t' = \frac{1}{2}(t_2 + t'_2)$ and temperature T can be found in Supplementary Note 5. According to the presence of altermagnetic order and energy gap, we identify three phases including altermagnetic insulator (AMI), altermagnetic metal (AMM) and paramagnetic metal (PM). The colors in Fig. 3a-c show the magnitude of the dimensionless altermagnetic order parameter,

which has a relation to the expectation value of spins per unit cell, $\frac{m_0}{U} = \frac{1}{3}\langle S^n \rangle$, where n represents the orientation of polarization.

The AMI phase is located at the weak SOC and strong interaction range in Fig. 3a. Its border shrinks rapidly with the increasing of λ_R . That is because Rashba SOC forces spins to deflect from the easy axis, frustrating the antiparallel sublattice alignment required for altermagnetic order. Besides, there is always an AMM phase between AMI and PM phases, where the altermagnetic order is partly established without a full energy gap. The irregular border shapes are attributed to numerical accuracy.

Nevertheless, SOC also breaks the $O(3)$ rotation symmetry of polarization in real space, making in-plane and out-of-plane orientations unequal. When spins are polarized in the plane, the deflecting effect is weakened due to geometric constraint, which is beneficial for establishing the altermagnetic order. Fig. 3b demonstrates that when θ is less than about 0.42, the magnetic phase transition occurs at a nearly constant $\lambda_R \approx 0.4$, and the AMM region is almost absent. As spins tilt toward the plane ($\theta \rightarrow \pi/2$), the altermagnetic region expands. The intermediate AMM phase, which possesses an indirect gap, also arises, implying the shift of energy bands.

We also investigate the influence of anisotropy in Fig. 3c. Varying δ only causes a modest change of phase borders compared to SOC. Larger anisotropy slightly favors the onset of altermagnetic order, extending the AMM region, but reduces the fully gapped AMI region. That is because the hopping of one direction is strengthened, enlarging not only band width but also band shift. We choose three line cuts to illustrate the process in Fig. 3d. The green curves trace the energy gap, while the purple curves show the order parameter. As δ increases, the slope of the $\frac{m_0}{U}$ curve decreases, and the AMM window gradually widens on both sides of the transition.

These phase diagrams underscore the competing role of SOC, which tends to destabilize antiparallel spin alignment, and anisotropy/polarization orientation, which can mitigate SOC-induced frustration, in forming the altermagnetic phases.

Chirality Switching of Spin Waves

To describe the collective magnetic excitations, we add a source term $S_H = \frac{1}{2} \int dx \bar{\Psi}(x) [\Gamma_{i3} H_e^i(x)] \Psi(x)$ to the action in spirit of the linear response theory. \vec{H}_e is an external magnetic field and has the same coupling formalism as \vec{m} . Within random phase approximation (RPA), we expand the effective action to the second order and take the derivative over source field \vec{H}_e twice. After some derivation (see Supplementary Note 4), the RPA retarded spin polarization function is

$$\Pi_{RPA,ij}^R = \Pi_{ij}^R (\delta_{ij} - \frac{U}{6} \Pi_{ij}^R)^{-1}, \quad (7)$$

where the bare polarization

$$\Pi_{ij}^R(x_1, x_2) = \frac{i}{2} \left(\text{Tr} [G^K(x_2, x_1) \Gamma_{i3} G^R(x_1, x_2) \Gamma_{j3}] + \text{Tr} [G^A(x_2, x_1) \Gamma_{i3} G^K(x_1, x_2) \Gamma_{j3}] \right) \quad (8)$$

encodes the particle-hole response with the Green's function of electrons. By defining the total spin operator $S^i = \frac{1}{2}\bar{\Psi}\Gamma_{i3}\Psi$, the retarded spin polarization function can also be expressed as $\Pi_{ij}^R(x_1, x_2) = i\theta(t_1 - t_2)\langle[S^i(x_1), S^j(x_2)]\rangle$. The poles of Eq. (7) are given by $f_{ij}(q, \omega) = \frac{U}{6}\Pi_{ij}^R - \delta_{ij} = 0$. When this condition is satisfied in an ordered phase, the polarization function diverges, indicating resonance of the response to an external perturbation. Low-frequency solutions of $f_{ij}(q, \omega) = 0$ determines the collective spin-wave modes (see Supplementary Note 6), whose dispersion can be extracted by searching ω at each q point. We fix the interaction strength at $U = 8$ to ensure the altermagnetic order, and numerically calculate two transverse propagating modes with opposite chirality, $\omega_R(q)$ and $\omega_L(q)$, corresponding to RH and LH precessional directions, respectively.

The dispersion of the RH and LH spin-wave modes is illustrated in Fig. 4a, which exhibits a novel chirality-splitting behavior. The two modes are fully split with $\omega_R > \omega_L$ in $\Gamma - (-M)$ range and $\omega_R < \omega_L$ in $\Gamma - M'$ range. However, they have relatively distinct slopes in $\Gamma - M$ and $\Gamma - (-M')$ ranges, making their order inverses on each side of the line crossings, which we may call chirality inversion, analogous to the spin inversion in electronic bands (Fig. 2c). There is also a crossing point between M and M' . Besides, several regions where we cannot find a real low-frequency solution appears around Γ , and they do not coincide for the two modes, thereby allowing nonreciprocal propagation, which means one chirality may propagate undamped while the other is forbidden. The static solutions $\omega = 0$ correspond to some $q \neq 0$ points, indicating spatially modulated ground states, which are beyond our scope here. Overall, the dispersion exhibits a C_{2x} symmetry.

In order to clarify the origin of such a chirality-splitting structure, we calculate the dispersion of the RH and LH modes under different conditions. When SOC is turned off (Fig. 4b), the complicated dispersion is reduced to a simple splitting effect with a higher $C_{4z}\mathcal{T}$ symmetry, originating from the pure altermagnetic crystalline anisotropy. Thus, the crossing point between M and M' is trivial because it actually lies on the high-symmetry path $\Gamma - Y$, where the energies of the two spin components are degenerate. The static solutions gather at Γ , implying a uniform ground state, in accordance with the spontaneous $SU(2)$ symmetry breaking by the altermagnetic order. Notably, although the result is calculated for x polarization, it is consistent with the z-polarized cases in Refs. [22, 25, 45], which again confirms the $O(3)$ symmetry of polarization. On the other hand, if we eliminate the hopping anisotropy while keep SOC (Fig. 4c), the RH and LH modes experience opposite shift towards $+q_y$ and $-q_y$ directions, respectively. As a consequence of the misplacement, the two modes split with $\omega_R < \omega_L$ in $q_y > 0$ region and $\omega_R > \omega_L$ in $q_y < 0$ region. The insoluble regions and spatially modulated ground states also originate from SOC. The overall symmetries are C_{2x} and M_y . In addition, when SOC and anisotropy both vanish (Fig. 4d), the system reduces to a conventional antiferromagnet, where the RH and LH modes are fully degenerate with the C_{4z} symmetry.

Therefore, the result in Fig. 4a is the superposition of splitting effect from altermagnetism and shifting effect from SOC, which can be traced back to the hybridization term in the electronic structure Eq. (6). Nevertheless, they respect distinct symmetries, leading to cooperative or competitive phenomena in different Brillouin zone sectors.

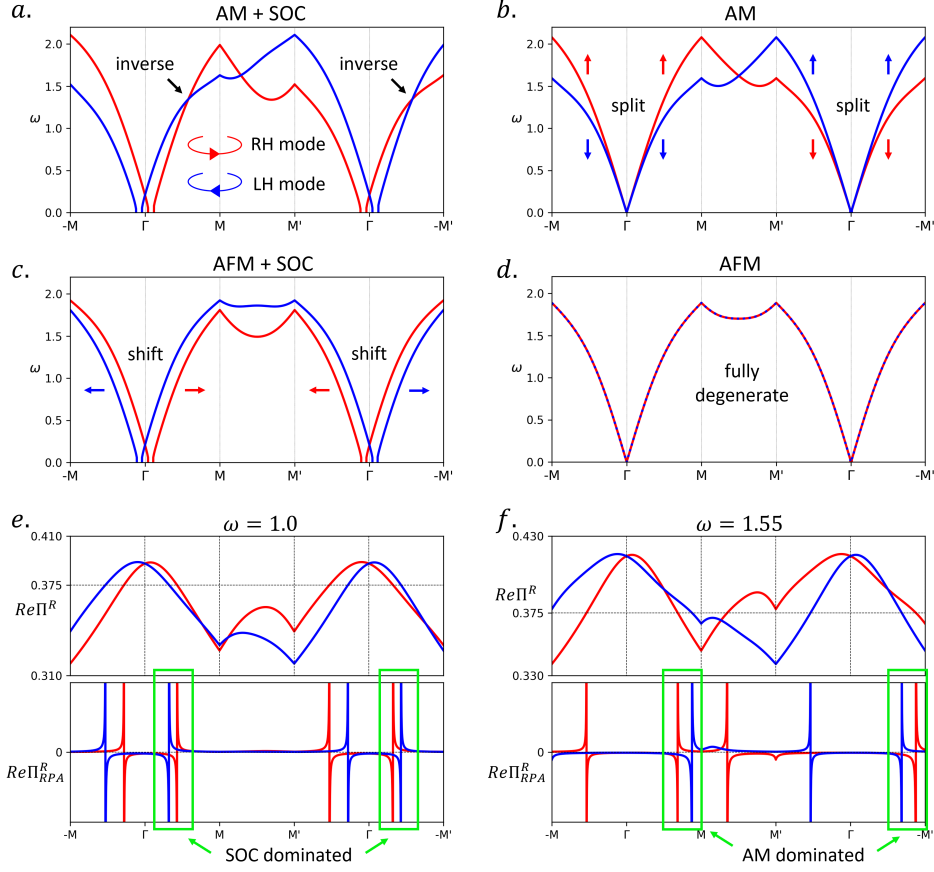


Fig. 4 Chirality splitting from different origins. **a-d** Dispersion of chiral spin waves under different conditions. **a** The two chiral modes of altermagnet (AM) with SOC exhibits novel chirality splitting. They are fully split along $\Gamma - (-M)$ and $\Gamma - M'$ directions while cross with each other along $\Gamma - M$ and $\Gamma - (-M')$ directions. **b** Without SOC, the crossing points disappear and the two modes split with a $C_{4z}\mathcal{T}$ symmetry due to crystalline anisotropy. **c** When the altermagnet is reduced to an antiferromagnet (AFM), the crossing points also vanish. SOC makes RH mode and LH mode shift towards opposite momentum directions, also resulting in chirality splitting. **d** In normal AFM, the RH and LH modes are fully degenerate. **e** The real part of bare and RPA polarization function at $\omega = 1.0$. The dotted line $\text{Re}\Pi^R = 0.375$ in the top subplot highlights the poles of RPA polarization function, corresponding to the resonance peaks in the bottom subplot. The relative position of RH and LH resonance peaks reflects SOC dominated chirality splitting around BZ center. **f** The real part of bare and RPA polarization function at $\omega = 1.55$. The relative position of resonance peaks is reversed compared to (e), indicating altermagnetism dominated chirality splitting around BZ edges.

Along $\Gamma - (-M)$ and $\Gamma - M'$ directions, they cooperate to enhance the chirality splitting, while the crossing points on $\Gamma - M$ and $\Gamma - (-M')$ originate from the competition. By comparison with Fig. 4b, c, it is explicit that SOC dominates the long-wave range and altermagnetism is more significant in the short-wave range instead. The crossing

points highlight the positions where the influence of SOC and altermagnetism cancels. Notably, for z polarization, the shifting effect of SOC is absent, and the dispersion reduces to a simple splitting structure, which is presented in Supplementary Note 7. Furthermore, we calculate the values of retarded spin polarization functions, Eq. (7) and Eq. (8). The top panels of Fig. 4e, f show that the bare polarization $\text{Re}\Pi^R$ is a slowly varying function of momentum and acquires its maximum value around Γ point. The intersections with $\text{Re}\Pi^R = 0.375$, corresponding to the resonant peaks of $\text{Re}\Pi_{RPA}^R$ in the bottom panels, indicate stable spin-wave responses to external excitations. For $\omega = 1.0$, the relative position of resonant peaks reveals SOC-dominated chirality splitting in the long-wave range, while for $\omega = 1.55$, the sequence is reversed, exhibiting altermagnetism-dominated structure.

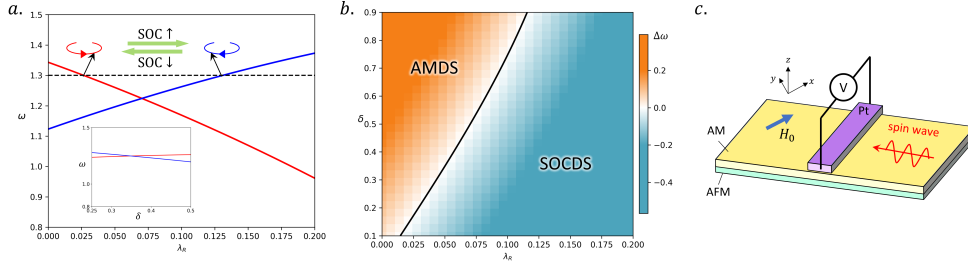


Fig. 5 SOC-driven chirality switching. **a** Frequency as the function of SOC strength λ_R and anisotropy δ (inset) for $q = (-\frac{\pi}{4}, \frac{\pi}{4})$. By increasing λ_R , the RH mode is switched to an LH mode while reversing λ_R switches it back. The inset picture shows that varying anisotropy has relatively weak influence. **b** Chirality hierarchy phase diagram. The altermagnetism-dominated splitting (AMDS) and SOC-dominated splitting (SOCDS) regions are separated by the solid line, on which the two modes are degenerate. Note that the λ_R axis is enlarged, reflecting the relatively strong effect of SOC. **c** Schematic of the experimental protocol. The altermagnetic film is interfaced with an antiferromagnetic layer, where a lateral electrical current induces Rashba SOC. An in-plane bias magnetic field polarizes spins along x-axis. The voltage signal in the Pt stripe reflects the chirality of spin waves.

Due to the opposite splitting hierarchies dominated by SOC and altermagnetism, the competition mechanism offers an approach to reversibly switch the chirality of spin waves through tuning SOC parameter. As shown in Fig. 5a, where we track the frequency of $q = (-\frac{\pi}{4}, \frac{\pi}{4})$ as a function of λ_R , the two chiral modes of $\omega = 1.3$ appear at different λ_R . If we fix the exciting frequency at $\omega = 1.3$, the altermagnet can hold an RH mode when $\lambda_R \approx 0.025$. Upon increasing λ_R to about 0.13, the RH mode is suppressed, and instead an LH mode is allowed. Decreasing λ_R switches it back, demonstrating reversible control of spin-wave chirality in altermagnets. The inset of Fig. 5a demonstrates that varying the anisotropy δ has smaller influence on the frequencies, which is an unfeasible way to switch the chirality. Furthermore, we calculate $\Delta\omega = \omega_R - \omega_L$ for $q = (-\frac{\pi}{4}, \frac{\pi}{4})$ across the parameter space to find the hierarchy phase diagram (Fig. 5b). The splitting structures in the two regions are dominated by SOC and altermagnetism, respectively, while on the boundary their influence cancels, resulting in degenerate chiral modes. Tuning the parameters across

the boundary may give us an opportunity for chirality switching with no need to vary the frequency and momentum. Notably, the enlarged λ_R axis implies a more significant effect of SOC. Therefore a very weak SOC is sufficient to satisfy the control requirement.

To validate the proposed SOC-driven chirality switching, we design an experiment platform (Fig. 5c) comprising an altermagnetic thin film heterostructured with an anti-ferromagnetic substrate, where a lateral electrical current can induce tunable Rashba SOC [28, 43]. An in-plane bias magnetic field is applied to fix spin polarization axis. The chirality of spin waves is detected by a Pt stripe on the top of the altermagnet, where the inverse spin Hall effect (ISHE) [27, 46–48] converts opposite chiralities into distinct voltage polarities. Initial resonant excitation by a right-circularly polarized laser with proper frequency generates an RH spin-wave mode [47–49], producing a characteristic ISHE voltage signal. Crucially, merely reversing the optical polarization excites an LH mode that rapidly damps out, yielding no detectable signal. Stabilization occurs only when enhanced SOC strength reaches a proper value, enabling the LH mode to manifest as reversed voltage polarity. This sequence provides unambiguous verification of active chirality control. Alternatively, chirality-resolved dispersion relations can be directly probed using heterodyne magneto-optic Kerr effect (HMOKE) microscopy [50]. The demonstrated chirality-switching capability enables the construction of chirality logic gates for ultrafast information processing, where binary states are encoded in spin-wave chiralities. By cascading such units within magnetic domain waveguides, all-electric spin-wave logic circuits can be realized, providing core components for next-generation spintronics.

Conclusion and Outlook

In conclusion, we proposed a novel mechanism for reversible switching of spin-wave chirality at specific frequency and momentum in altermagnets, achieved through tuning SOC strength. Theoretical investigations revealed that momentum-dependent competition between SOC and altermagnetism generates opposing chirality-splitting structures in distinct Brillouin zone regions, establishing the physical foundation for SOC-driven chirality switching. Although spin-wave chirality switching has been explored in ferrimagnets [51, 52], altermagnets offer a fundamentally advantageous platform, due to their vanishing net magnetization and intrinsic chirality splitting [22, 25, 45], making them ideal hosts for chirality-bit implementations. Our work establishes a theoretical framework for SOC-mediated control of chiral excitations and enables active switching of binary chirality states. This chirality-bit manipulation paradigm paves the way for ultrafast, low-consumption, fully electric-field-controlled spin-wave logic devices, thereby advancing the development of chirality-based spintronics.

Supplementary information. The online version contains supplementary material available at xxx.

Acknowledgements. W.T.Li and W.M.Liu are supported by the National Key R&D Program of China under Grants No. 2024YFF0726700, 2021YFA1400900 and 2021YFA0718300, NSFC under Grants No. 12334012, 12234012, 52327808 and

12174461, and the Space Application System of China Manned Space Program. J.T.Wang acknowledges the financial support from the NSFC under Grants No. 92263202 and 12374020, the National Key R&D Program of China under Grant No. 2020YFA0711502, and the Strategic Priority Research Program of the Chinese Academy of Sciences under Grant No. XDB33000000.

References

- [1] L. Šmejkal, J. Sinova, T. Jungwirth, Beyond conventional ferromagnetism and antiferromagnetism: A phase with nonrelativistic spin and crystal rotation symmetry. *Physical Review X* **12**(3), 031042 (2022). <https://doi.org/10.1103/PhysRevX.12.031042>
- [2] L. Šmejkal, J. Sinova, T. Jungwirth, Emerging research landscape of altermagnetism. *Physical Review X* **12**(4), 040501 (2022). <https://doi.org/10.1103/PhysRevX.12.040501>
- [3] J. Krempaský, L. Šmejkal, S.W. D’Souza, M. Hajlaoui, G. Springholz, K. Uhlířová, F. Alarab, P.C. Constantinou, V. Strocov, D. Usanov, W.R. Pudelko, R. González-Hernández, A. Birk Hellenes, Z. Jansa, H. Reichlová, Z. Šobáň, R.D. Gonzalez Betancourt, P. Wadley, J. Sinova, D. Kriegner, J. Minár, J.H. Dil, T. Jungwirth, Altermagnetic lifting of kramers spin degeneracy. *Nature* **626**(7999), 517–522 (2024). <https://doi.org/10.1038/s41586-023-06907-7>
- [4] Y.P. Zhu, X. Chen, X.R. Liu, Y. Liu, P. Liu, H. Zha, G. Qu, C. Hong, J. Li, Z. Jiang, X.M. Ma, Y.J. Hao, M.Y. Zhu, W. Liu, M. Zeng, S. Jayaram, M. Lenger, J. Ding, S. Mo, K. Tanaka, M. Arita, Z. Liu, M. Ye, D. Shen, J. Wrachtrup, Y. Huang, R.H. He, S. Qiao, Q. Liu, C. Liu, Observation of plaid-like spin splitting in a noncoplanar antiferromagnet. *Nature* **626**(7999), 523–528 (2024). <https://doi.org/10.1038/s41586-024-07023-w>
- [5] S. Lee, S. Lee, S. Jung, J. Jung, D. Kim, Y. Lee, B. Seok, J. Kim, B.G. Park, L. Šmejkal, C.J. Kang, C. Kim, Broken kramers degeneracy in altermagnetic mnte. *Physical Review Letters* **132**(3), 036702 (2024). <https://doi.org/10.1103/PhysRevLett.132.036702>
- [6] S. Reimers, L. Odenbreit, L. Šmejkal, V.N. Strocov, P. Constantinou, A.B. Hellenes, R. Jaeschke Ubierno, W.H. Campos, V.K. Bharadwaj, A. Chakraborty, T. Denneulin, W. Shi, R.E. Dunin-Borkowski, S. Das, M. Kläui, J. Sinova, M. Jourdan, Direct observation of altermagnetic band splitting in crsb thin films. *Nature Communications* **15**(1), 2116 (2024). <https://doi.org/10.1038/s41467-024-46476-5>
- [7] M. Zeng, M.Y. Zhu, Y.P. Zhu, X.R. Liu, X.M. Ma, Y.J. Hao, P. Liu, G. Qu, Y. Yang, Z. Jiang, K. Yamagami, M. Arita, X. Zhang, T.H. Shao, Y. Dai, K. Shimada, Z. Liu, M. Ye, Y. Huang, Q. Liu, C. Liu, Observation of spin splitting

- in room-temperature metallic antiferromagnet *crsb*. *Advanced Science* **11**(43), 2406529 (2024). <https://doi.org/10.1002/advs.202406529>
- [8] B. Jiang, M. Hu, J. Bai, Z. Song, C. Mu, G. Qu, W. Li, W. Zhu, H. Pi, Z. Wei, Y.J. Sun, Y. Huang, X. Zheng, Y. Peng, L. He, S. Li, J. Luo, Z. Li, G. Chen, H. Li, H. Weng, T. Qian, A metallic room-temperature d-wave altermagnet. *Nature Physics* pp. 1–6 (2025). <https://doi.org/10.1038/s41567-025-02822-y>
 - [9] P. Das, V. Leeb, J. Knolle, M. Knap, Realizing altermagnetism in fermi-hubbard models with ultracold atoms. *Physical Review Letters* **132**(26), 263402 (2024). <https://doi.org/10.1103/PhysRevLett.132.263402>
 - [10] C.T. Liao, Y.C. Wang, Y.C. Tien, S.Y. Huang, D. Qu, Separation of inverse altermagnetic spin-splitting effect from inverse spin hall effect in ruo 2. *Physical Review Letters* **133**(5), 056701 (2024). <https://doi.org/10.1103/PhysRevLett.133.056701>
 - [11] M. Gu, Y. Liu, H. Zhu, K. Yananose, X. Chen, Y. Hu, A. Stroppa, Q. Liu, Ferroelectric switchable altermagnetism. *Physical Review Letters* **134**(10), 106802 (2025). <https://doi.org/10.1103/PhysRevLett.134.106802>
 - [12] C. Song, H. Bai, Z. Zhou, L. Han, H. Reichlova, J.H. Dil, J. Liu, X. Chen, F. Pan, Altermagnets as a new class of functional materials. *Nature Reviews Materials* pp. 1–13 (2025). <https://doi.org/10.1038/s41578-025-00779-1>
 - [13] R. González-Hernández, L. Šmejkal, K. Výborný, Y. Yahagi, J. Sinova, T. Jungwirth, J. Železný, Efficient electrical spin splitter based on nonrelativistic collinear antiferromagnetism. *Physical Review Letters* **126**(12), 127701 (2021). <https://doi.org/10.1103/PhysRevLett.126.127701>
 - [14] Y. Zhang, H. Bai, L. Han, C. Chen, Y. Zhou, C.H. Back, F. Pan, Y. Wang, C. Song, Simultaneous high charge-spin conversion efficiency and large spin diffusion length in altermagnetic ruo2. *Advanced Functional Materials* **34**(24), 2313332 (2024). <https://doi.org/10.1002/adfm.202313332>
 - [15] Y. Guo, J. Zhang, Z. Zhu, Y.y. Jiang, L. Jiang, C. Wu, J. Dong, X. Xu, W. He, B. He, Z. Huang, L. Du, G. Zhang, K. Wu, X. Han, D.f. Shao, G. Yu, H. Wu, Direct and inverse spin splitting effects in altermagnetic ruo2. *Advanced Science* **11**(25), 2400967 (2024). <https://doi.org/10.1002/advs.202400967>
 - [16] X. Zhou, W. Feng, X. Yang, G.Y. Guo, Y. Yao, Crystal chirality magneto-optical effects in collinear antiferromagnets. *Physical Review B* **104**(2), 024401 (2021). <https://doi.org/10.1103/PhysRevB.104.024401>
 - [17] L. Han, X. Fu, R. Peng, X. Cheng, J. Dai, L. Liu, Y. Li, Y. Zhang, W. Zhu, H. Bai, Y. Zhou, S. Liang, C. Chen, Q. Wang, X. Chen, L. Yang, Y. Zhang, C. Song, J. Liu, F. Pan, Electrical 180° switching of néel vector in spin-splitting

- antiferromagnet. *Science Advances* **10**(4), eadn0479 (2024). <https://doi.org/10.1126/sciadv.adn0479>
- [18] L. Šmejkal, A.B. Hellenes, R. González-Hernández, J. Sinova, T. Jungwirth, Giant and tunneling magnetoresistance in unconventional collinear antiferromagnets with nonrelativistic spin-momentum coupling. *Physical Review X* **12**(1), 011028 (2022). <https://doi.org/10.1103/PhysRevX.12.011028>
 - [19] F. Liu, Z. Zhang, X. Yuan, Y. Liu, S. Zhu, Z. Lu, R. Xiong, Giant tunneling magnetoresistance in insulated altermagnet/ferromagnet junctions induced by spin-dependent tunneling effect. *Physical Review B* **110**(13), 134437 (2024). <https://doi.org/10.1103/PhysRevB.110.134437>
 - [20] X. Zhou, W. Feng, R.W. Zhang, L. Šmejkal, J. Sinova, Y. Mokrousov, Y. Yao, Crystal thermal transport in altermagnetic ruo 2. *Physical Review Letters* **132**(5), 056701 (2024). <https://doi.org/10.1103/PhysRevLett.132.056701>
 - [21] S. Das, A. Ross, X.X. Ma, S. Becker, C. Schmitt, F. van Duijn, E.F. Galindez-Ruales, F. Fuhrmann, M.A. Syskaki, U. Ebels, V. Baltz, A.L. Barra, H.Y. Chen, G. Jakob, S.X. Cao, J. Sinova, O. Gomonay, R. Lebrun, M. Kläui, Anisotropic long-range spin transport in canted antiferromagnetic orthoferite yfeo3. *Nature Communications* **13**(1), 6140 (2022). <https://doi.org/10.1038/s41467-022-33520-5>
 - [22] L. Šmejkal, A. Marmodoro, K.H. Ahn, R. González-Hernández, I. Turek, S. Mankovsky, H. Ebert, S.W. D'Souza, O. Šipr, J. Sinova, T. Jungwirth, Chiral magnons in altermagnetic RuO_2 . *Physical Review Letters* **131**(25), 256703 (2023). <https://doi.org/10.1103/PhysRevLett.131.256703>
 - [23] Q. Cui, B. Zeng, P. Cui, T. Yu, H. Yang, Efficient spin seebeck and spin nernst effects of magnons in altermagnets. *Physical Review B* **108**(18), L180401 (2023). <https://doi.org/10.1103/PhysRevB.108.L180401>
 - [24] E.W. Hodt, J. Linder, Spin pumping in an altermagnet/normal-metal bilayer. *Physical Review B* **109**(17), 174438 (2024). <https://doi.org/10.1103/PhysRevB.109.174438>
 - [25] Z. Liu, M. Ozeki, S. Asai, S. Itoh, T. Masuda, Chiral split magnon in altermagnetic mnte. *Physical Review Letters* **133**(15), 156702 (2024). <https://doi.org/10.1103/PhysRevLett.133.156702>
 - [26] H. Wang, H. Yu, Perspectives on antiferromagnetic magnonics. *Science Bulletin* **69**(21), 3324–3328 (2024). <https://doi.org/10.1016/j.scib.2024.09.007>
 - [27] L. Sheng, A. Duvakina, H. Wang, K. Yamamoto, R. Yuan, J. Wang, P. Chen, W. He, K. Yu, Y. Zhang, J. Chen, J. Hu, W. Song, S. Liu, X. Han, D. Yu, J.P. Ansermet, S. Maekawa, D. Grundler, H. Yu, Control of spin currents by

- magnon interference in a canted antiferromagnet. *Nature Physics* pp. 1–6 (2025). <https://doi.org/10.1038/s41567-025-02819-7>
- [28] A. Manchon, J. Železný, I.M. Miron, T. Jungwirth, J. Sinova, A. Thiaville, K. Garello, P. Gambardella, Current-induced spin-orbit torques in ferromagnetic and antiferromagnetic systems. *Reviews of Modern Physics* **91**(3), 035004 (2019). <https://doi.org/10.1103/RevModPhys.91.035004>
 - [29] P. Wadley, B. Howells, J. Železný, C. Andrews, V. Hills, R.P. Campion, V. Novák, K. Olejník, F. Maccherozzi, S.S. Dhesi, S.Y. Martin, T. Wagner, J. Wunderlich, F. Freimuth, Y. Mokrousov, J. Kuneš, J.S. Chauhan, M.J. Grzybowski, A.W. Rushforth, K.W. Edmonds, B.L. Gallagher, T. Jungwirth, Electrical switching of an antiferromagnet. *Science* **351**(6273), 587–590 (2016). <https://doi.org/10.1126/science.aab1031>
 - [30] W.X. Guo, Y.H. Chen, L. Zhuang, W.M. Liu, First-order metal–ferromagnetic insulator phase transition induced by rashba spin-orbit coupling on the puckered honeycomb lattice. *Journal of Physics: Condensed Matter* **33**(33), 335603 (2021). <https://doi.org/10.1088/1361-648X/ac0a1d>
 - [31] S. Calder, J.G. Vale, N.A. Bogdanov, X. Liu, C. Donnerer, M.H. Upton, D. Casa, A.H. Said, M.D. Lumsden, Z. Zhao, J.Q. Yan, D. Mandrus, S. Nishimoto, J. van den Brink, J.P. Hill, D.F. McMorrow, A.D. Christianson, Spin-orbit-driven magnetic structure and excitation in the 5d pyrochlore $\text{Cd}_2\text{Os}_2\text{O}_7$. *Nature Communications* **7**(1), 11651 (2016). <https://doi.org/10.1038/ncomms11651>
 - [32] X. Gui, S. Calder, H. Cao, T. Yu, W. Xie, Geometric and magnetic structures of K_2ReI_6 as an antiferromagnetic insulator with ferromagnetic spin-canting originated from spin-orbit coupling. *The Journal of Physical Chemistry C* **123**(3), 1645–1652 (2019). <https://doi.org/10.1021/acs.jpcc.8b11371>
 - [33] J. Sinova, S.O. Valenzuela, J. Wunderlich, C.H. Back, T. Jungwirth, Spin hall effects. *Reviews of Modern Physics* **87**(4), 1213–1260 (2015). <https://doi.org/10.1103/RevModPhys.87.1213>
 - [34] F. Sun, J. Ye, W.M. Liu. Quantum incommensurate skyrmion crystals and commensurate to in-commensurate transitions in cold atoms and materials with spin orbit couplings in a zeeman field (2017). <https://doi.org/10.48550/arXiv.1502.05338>
 - [35] L. Šmejkal, A.H. MacDonald, J. Sinova, S. Nakatsuji, T. Jungwirth, Anomalous hall antiferromagnets. *Nature Reviews Materials* **7**(6), 482–496 (2022). <https://doi.org/10.1038/s41578-022-00430-3>
 - [36] H. Reichlova, R. Lopes Seeger, R. González-Hernández, I. Kounta, R. Schlitz, D. Kriegner, P. Ritzinger, M. Lammel, M. Leiviskä, A. Birk Hellenes, K. Olejník, V. Petříček, P. Doležal, L. Horak, E. Schmoranzero, A. Badura, S. Bertaina,

- A. Thomas, V. Baltz, L. Michez, J. Sinova, S.T.B. Goennenwein, T. Jungwirth, L. Šmejkal, Observation of a spontaneous anomalous hall response in the mn_5si_3 d-wave altermagnet candidate. *Nature Communications* **15**(1), 4961 (2024). <https://doi.org/10.1038/s41467-024-48493-w>
- [37] P.J. Guo, Z.X. Liu, Z.Y. Lu, Quantum anomalous hall effect in collinear antiferromagnetism. *npj Computational Materials* **9**(1), 1–6 (2023). <https://doi.org/10.1038/s41524-023-01025-4>
- [38] T. Sato, S. Haddad, I.C. Fulga, F.F. Assaad, J. Van Den Brink, Altermagnetic anomalous hall effect emerging from electronic correlations. *Physical Review Letters* **133**(8), 086503 (2024). <https://doi.org/10.1103/PhysRevLett.133.086503>
- [39] K.D. Belashchenko, Giant strain-induced spin splitting effect in mnTe, a g -wave altermagnetic semiconductor. *Physical Review Letters* **134**(8), 086701 (2025). <https://doi.org/10.1103/PhysRevLett.134.086701>
- [40] R.D. Gonzalez Betancourt, J. Zubáč, R. Gonzalez-Hernandez, K. Geishendorf, Z. Šobáň, G. Springholz, K. Olejník, L. Šmejkal, J. Sinova, T. Jungwirth, S.T.B. Goennenwein, A. Thomas, H. Reichlová, J. Železný, D. Kriegner, Spontaneous anomalous hall effect arising from an unconventional compensated magnetic phase in a semiconductor. *Physical Review Letters* **130**(3), 036702 (2023). <https://doi.org/10.1103/PhysRevLett.130.036702>
- [41] P. Liu, J. Li, J. Han, X. Wan, Q. Liu, Spin-group symmetry in magnetic materials with negligible spin-orbit coupling. *Physical Review X* **12**(2), 021016 (2022). <https://doi.org/10.1103/PhysRevX.12.021016>
- [42] Y. Fang, J. Cano, S.A.A. Ghorashi, Quantum geometry induced nonlinear transport in altermagnets. *Physical Review Letters* **133**(10), 106701 (2024). <https://doi.org/10.1103/PhysRevLett.133.106701>
- [43] J. Železný, H. Gao, K. Výborný, J. Zemen, J. Mašek, A. Manchon, J. Wunderlich, J. Sinova, T. Jungwirth, Relativistic néel-order fields induced by electrical current in antiferromagnets. *Physical Review Letters* **113**(15), 157201 (2014). <https://doi.org/10.1103/PhysRevLett.113.157201>
- [44] K. Ishiwata, Axion mass in antiferromagnetic insulators. *Physical Review D* **104**(1), 016004 (2021). <https://doi.org/10.1103/PhysRevD.104.016004>
- [45] T.A. Maier, S. Okamoto, Weak-coupling theory of neutron scattering as a probe of altermagnetism. *Physical Review B* **108**(10), L100402 (2023). <https://doi.org/10.1103/PhysRevB.108.L100402>
- [46] M. Balinskiy, H. Chiang, D. Gutierrez, A. Khitun, Spin wave interference detection via inverse spin hall effect. *Applied Physics Letters* **118**(24), 242402 (2021). <https://doi.org/10.1063/5.0055402>

- [47] J. Li, C.B. Wilson, R. Cheng, M. Lohmann, M. Kavand, W. Yuan, M. Aldosary, N. Agladze, P. Wei, M.S. Sherwin, J. Shi, Spin current from sub-terahertz-generated antiferromagnetic magnons. *Nature* **578**(7793), 70–74 (2020). <https://doi.org/10.1038/s41586-020-1950-4>
- [48] P. Vaidya, S.A. Morley, J. van Tol, Y. Liu, R. Cheng, A. Brataas, D. Lederman, E. del Barco, Subterahertz spin pumping from an insulating antiferromagnet. *Science* **368**(6487), 160–165 (2020). <https://doi.org/10.1126/science.aaz4247>
- [49] J.R. Hortensius, D. Afanasiev, M. Matthiesen, R. Leenders, R. Citro, A.V. Kimel, R.V. Mikhaylovskiy, B.A. Ivanov, A.D. Caviglia, Coherent spin-wave transport in an antiferromagnet. *Nature Physics* **17**(9), 1001–1006 (2021). <https://doi.org/10.1038/s41567-021-01290-4>
- [50] D. Hayashi, Y. Shiotani, M. Ishibashi, R. Hisatomi, T. Moriyama, T. Ono, Observation of mode splitting by magnon–magnon coupling in synthetic antiferromagnets. *Applied Physics Express* **16**(5), 053004 (2023). <https://doi.org/10.35848/1882-0786/acd5a6>
- [51] L. Wang, L. Shen, H. Bai, H.A. Zhou, K. Shen, W. Jiang, Electrical excitation and detection of chiral magnons in a compensated ferrimagnetic insulator. *Physical Review Letters* **133**(16), 166705 (2024). <https://doi.org/10.1103/PhysRevLett.133.166705>
- [52] Y. Liu, Z. Xu, L. Liu, K. Zhang, Y. Meng, Y. Sun, P. Gao, H.W. Zhao, Q. Niu, J. Li, Switching magnon chirality in artificial ferrimagnet. *Nature Communications* **13**(1), 1264 (2022). <https://doi.org/10.1038/s41467-022-28965-7>